Hyperbolic Uncertainty Aware Semantic Segmentation

Bike Chen, Wei Peng, Xiaofeng Cao, Juha Röning

***Abstract*—Semantic segmentation (SS) aims to classify each pixel into one of the pre-defined classes. This task plays an important role in self-driving cars and autonomous drones. In SS, many works have shown that most misclassified pixels are commonly near object boundaries with high uncertainties. However, existing SS loss functions are not tailored to handle these uncertain pixels during training, as these pixels are usually treated equally as confidently classified pixels and cannot be embedded with arbitrary low distortion in Euclidean space, thereby degenerating the performance of SS. To overcome this problem, this paper designs a "Hyperbolic Uncertainty Loss" (HyperUL), which dynamically highlights the misclassified and high-uncertainty pixels in Hyperbolic space during training via the hyperbolic distances. The proposed HyperUL is model agnostic and can be easily applied to various neural architectures. After employing HyperUL to three recent SS models, the experimental results on Cityscapes and UAVid datasets reveal that the segmentation performance of existing SS models can be consistently improved.**

***Index Terms*—Hyperbolic Space, Hyperbolic Uncertainty, Semantic Segmentation, Self-driving Cars, Autonomous Drones.**

I. Introduction

SEMANTIC segmentation (SS) separates an image into different meaningful and coherent parts to identify distinct objects. Hence it can serve as a powerful and practical tool for the further image analysis [1], [2] such as scene categorization, and free space detection. Apparently, high segmentation performance in autonomous vehicles or autonomous drones will help comprehensively understand the surrounding environment, hence greatly improving the safety [3].

Although most existing SS models have achieved impressive segmentation performance, they did not utilize uncertainty information during training. Uncertainty indicates whether a pixel in an image will be classified confidently or not. Improving uncertain predictions can improve segmentation performance, as uncertain predictions are strongly related to misclassifications of pixels. As depicted in Fig. 1, uncertain pixels contain a large number of misclassified pixels, *i.e.*, green pixels. It means that improving uncertain predictions also corrects wrong predictions. There exist a few works exploring this direction. For example, the works [5] and [6], [7] used Monte Carlo Dropout and Deep Ensembles to estimate uncertainties and improve segmentation outputs. However, these methods are computational overhead and they did not consider uncertainty during training. These works [8], [9] took uncertainty in the training stage. However, [8] only considered the uncertainty of the class by assigning different weights to different classes, not to each pixel. [9] intended to reduce the impact of uncertainty by giving each uncertain pixel a fixed small weight. In this paper, we argue that weighting each uncertain pixel dynamically during training might improve segmentation performance.

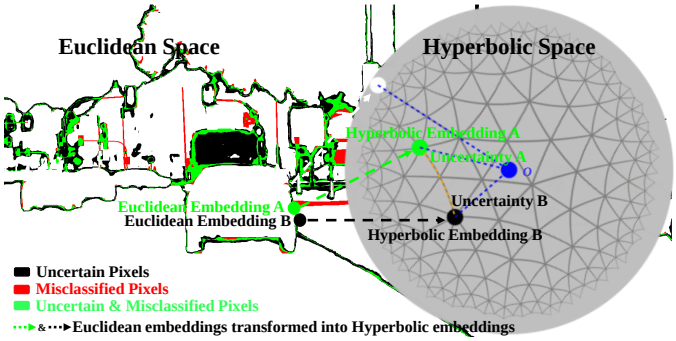

Fig. 1. **Left side:** Uncertainties visualization of an image from the Cityscapes dataset [1]. Uncertain pixels (*i.e.*, black and green pixels) are near object boundaries. Not shown pixels means that they are classified certainly with more than 95 percentile. **Right side:** The silver circle indicates the Poincaré Ball model of Hyperbolic space. The hyperbolic distance (*i.e.*, blue dashed lines) from the hyperbolic embedding (*e.g.*, Hyperbolic Embedding A or B) to the origin (*i.e.*, blue point) can serve as an estimate of uncertainty [4]. After all embeddings of pixels are transformed from Euclidean space into Hyperbolic space (*e.g.*, Euclidean Embedding A and B to corresponding Hyperbolic Embedding A and B), uncertainty weights will be calculated and then dynamically applied to these transformed pixels.

Uncertain pixels are commonly near object boundaries. However, existing SS models have not the natural ability to distinguish these pixels only based on Euclidean embeddings, as hierarchical structures cannot be embedded with arbitrary low distortion in Euclidean space even with an unbounded number of dimensions [10]. We argue that segmentation datasets exhibit latent hierarchical structures, and thus can benefit from embedding in hyperbolic space. Here, we provide an observation and quantification analysis to verify this. To achieve better segmentation performance, containing rich contextual information for each pixel embedding is extremely important. The contextual information is commonly aggregated by modeling the long-range dependencies among pixels. Therefore, a pixel embedding, especially for a pixel on the boundary, might be contributed by other pixels from totally different classes. This means that embedding a pixel is similar to embedding a hierarchy. In addition, we further verify that there exist hierarchical structures in segmentation data by

B. Chen, J. Röning are with the Biomimetics and Intelligent Systems Group, and W. Peng is with the Center for Machine Vision and Signal Analysis, University of Oulu, Oulu, Finland. X.F. Cao is with the School of Artificial Intelligence, Jilin University, Changchun, China. (e-mail: {Bike.Chen, Wei.Peng, Juha.Roning}@oulu.fi, xiaofeng.cao.uts@gmail.com)

Corresponding author: Juha Röning.

δ-hyperbolicity [4]. The δ-hyperbolicity can be utilized to measure the data structure similarity between Euclidean space and Hyperbolic space. The δ-hyperbolicity is in $[0, 1]$. When the calculated δ-hyperbolicty on a data set is closer to 0, the degree of hyperbolicity of the data is quite high. This means that there exists strong hierarchy in the data. In contrast, the computed δ-hyperbolicity closer to 1 indicates that there is no hierarchy in the dataset. Taking Cityscapes [1] and UAVid [11] for examples, in Table I, we see that these two datasets are with strong hierarchical structures, since δ-hyperbolicity 0.16 is closer to 0.

TABLE I
THEORETICAL δ-HYPERBOLICITY AND REAL δ-HYPERBOLICITY VALUES IN CITYSCAPES AND UAVID DATASETS. $\mathbb{B}^n$ IS THE POINCARÉ BALL MODEL OF HYPERBOLIC SPACE.

Spaces	$\mathbb{B}^n$
Theory	0
Cityscapes dataset (δ)	0.16
UAVid dataset (δ)	0.16

Our Method. To cope with this problem, we first turn to Hyperbolic space [4], [12] to better model the underlying hierarchical structures, as exponentially expanding Hyperbolic space has the innate ability to capture the structures of segmentation data. Then we adopt the uncertainty information during training to improve the performance of SS. To achieve this goal, we introduce the "Hyperbolic Uncertainty Loss" (HyperUL), which dynamically emphasizes the misclassified and not confidently classified pixels in the training phase. Specifically, as shown in Fig. 1, we first transform the embeddings of the last layer of trained SS models from Euclidean space into Hyperbolic space. Then HyperUL is appended to the transformed embeddings during training, and dynamically assigns distinct weights to different pixels by the calculated hyperbolic distances. Uncertain pixels whose embeddings are closer to the origin will obtain larger weights and vice versa.

In order to take full advantage of the proposed HyperUL, we provide various implementations such as HyperUL-CE, HyperUL-OHEM, and HyperUL-CE-OHEM. HyperUL-CE is the combination of uncertainty weights with cross-entropy loss. HyperUL-OHEM behaves like Online Hard Example Mining (OHEM) [13], and picks higher uncertain pixels for back-propagation during training. HyperUL-CE-OHEM is the combination of HyperUL-CE and HyperUL-OHEM. It first uses uncertainty weights to scale cross-entropy loss and then selects higher uncertain pixels for back-propagation. For the ease of descriptions in the following content, we use the name of HyperUL to indicate all variants.

To validate the effectiveness of our proposed HyperUL, we replace the cross-entropy loss or cross-entropy loss combined with OHEM by our proposed loss function on recently representative deep learning methods [14]–[16]. The experimental results on Cityscapes and UAVid datasets demonstrate that by employing HyperUL, most existing SS models can consistently obtain segmentation performance improvement.

Our Contributions. The contributions of this paper are as follows:

(1) We propose HyperUL, which can improve SS performance by considering hyperbolic uncertainty information during training. To the best of our knowledge, this is the first paper to explore hyperbolic uncertainty in the supervised SS task.

(2) To fully take the advantages of hyperbolic uncertainty information, we provide three specific implementations, *i.e.*, HyperUL-CE, HyperUL-OHEM, and HyperUL-CE-OHEM. We also provide detailed ablation studies for them.

(3) We provide comparison experiments between the proposed loss and baseline losses (*i.e.*, cross-entropy loss or cross-entropy loss combined with OHEM) on both Cityscapes and UAVid datasets. With the proposed HyperUL, existing SS models achieve additional segmentation performance improvement.

The rest of this paper is organized as follows. In Section II, we review related works. After that, we provide basics of Poincaré Ball model in Section III. In Section IV, we detail our proposed HyperUL and various variants. In Section V, we provide the experimental results on Cityscapes and UAVid datasets. Finally, we conclude our paper in Section VI.

II. RELATED WORK

In this section, we first introduce recent semantic segmentation methods, then Hyperbolic space related works, and finally uncertainty relevant approaches.

Semantic Segmentation. Recent works [15]–[18] focus on the design of real-time and high-performance semantic segmentation (SS) models. For instance, the paper [15] designed a two-branch neural network, which simultaneously captures low-level details and obtains high-level semantic context to achieve a perfect speed-accuracy tradeoff. The work [16] inherited the desirable properties of BiSeNetV2, but adopted a detail guidance module to enforce the proposed SS model to learn spatial features directly instead of adding an extra branch. Building a long-range dependencies or capturing global context information plays a key role in SS models. These works [14], [19]–[21] adopted various Transformer techniques to encode global contextual features to achieve better segmentation performances. For example, SegFormer [14] incorporated Transformer modules and lightweight multi-layer perception decoders in the design of the SS model. HRFormer [21] introduced a local-window self-attention in HRNet [22] to improve segmentation efficiency and performance. Although these networks have achieved high performances, they are only considered in Euclidean space and do not take the uncertainties of segmentation results into consideration. Hence, this work proposes HyperUL, which is in Hyperbolic space and incorporates the uncertainties in training SS models. With the proposed HyperUL, most existing SS models could achieve better performance.

Hyperbolic Space. Due to the outstanding ability of modeling the underlying hierarchical structure of datasets, Hyperbolic space [4], [12], [23], [24] has recently attracted increasing attention in the fields of Natural Language Processing (NLP) and Computer Vision (CV). These two works [23], [24] tried to create corresponding hyperbolic neural

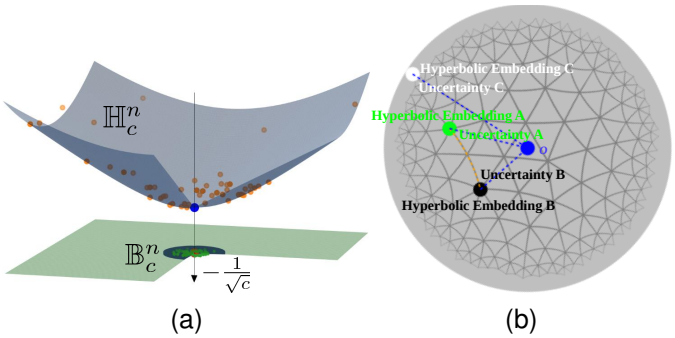

Fig. 2. (a) The geometric relationship between Hyperboloid model $\mathbb{H}_c^n$ and Poincaré Ball model $\mathbb{B}_c^n$. The Poincaré Ball model $\mathbb{B}_c^n$ is the projection of the Hyperboloid model onto the n-dimensional space-like hyperplane (*i.e.*, the blue circle in the light green plane). (b) is the enlarged space-like hyperplane. For the Poincaré Ball model in Hyperbolic space, the hyperbolic distances from hyperbolic embeddings A, B, and C to the origin o can serve as the measure of uncertainty of pixels A, B, and C, respectively.

network operations to build pure hyperbolic neural networks in NLP. These papers [4], [25], [26] demonstrated that in some practical CV applications, hyperbolic embeddings would be a better alternative compared with Euclidean and spherical embeddings. However, to the best of our knowledge, there are no researchers who have explored this potential direction in the supervised SS task. Our work is the first paper to apply hyperbolic properties in this task.

Uncertainty. For deep learning models, providing certainty estimates plays an important role in safety-critical real world applications, such as medical image analysis and autonomous vehicle control. Many methods [5], [6], [27]–[29] such as Bayesian inference, deep ensembles, and single deterministic networks, have been proposed for modeling data uncertainty (*i.e.*, aleatoric uncertainty) and model uncertainty (*i.e.*, epistemic uncertainty), and further to improve segmentation performance. However, these methods are usually computational overhead and they did not handle uncertainty during training. Although these works [8], [9] took uncertainty in the training stage, [8] only considered the uncertainty of the class, not every single pixel, and [9] intended to reduce the impact of uncertainty, not utilizing the uncertainty. In contrast, we use the hyperbolic distance to efficiently estimate the uncertainty of each pixel, and then adopt the calculated uncertainties as weights to operate on these pixels during training.

III. Basics of Poincaré Ball Model

In this section, we first briefly introduce Hyperbolic space, and then introduce the definition of Poincaré Ball model, and finally introduce commonly used operations in the Poincaré Ball model.

Hyperbolic Space. A Hyperbolic space is defined by a Riemannian manifold with a constant negative curvature. There are five isometric models and the most basic model is an n-dimensional Hyperboloid model with a hypersurface $\mathbb{H}_c^n$, as depicted in Fig. 2a. The Poincaré Ball model $\mathbb{B}_c^n$ is a projection of the Hyperboloid model onto the n-dimensional space-like hyperplane.

Poincaré Ball Model. An n-dimensional Poincaré Ball model with a constant sectional curvature $-c$ is defined as $(\mathbb{B}_c^n, \mathfrak{g}^c)$, where $\mathbb{B}_c^n = \{\boldsymbol{x} \in \mathbb{R}^n \mid c\|\boldsymbol{x}\| < 1\}$ is the Hyperbolic space and $\mathfrak{g}_{\boldsymbol{x}}^c = (\lambda_{\boldsymbol{x}}^c)^2 \boldsymbol{I}_n$ is the corresponding metric tensor at the point $\boldsymbol{x}$. $\lambda_{\boldsymbol{x}}^c$ is the conformal factor defined as $\lambda_{\boldsymbol{x}}^c = 2\left(1 - c\|\boldsymbol{x}\|^2\right)^{-1}$. $\boldsymbol{I}_n$ is the Euclidean metric tensor.

The $c^{-\frac{1}{2}}$ is the radius of Poincaré Ball. Same as previous works [23], [24], we adopt the formalism of Möbius gyrovector space [30] to provide basic Euclidean-like operations.

Möbius Addition. For $\forall \boldsymbol{x} \in \mathbb{B}_c^n$ and $\forall \boldsymbol{y} \in \mathbb{B}_c^n$, the Möbius addition is defined as follows:

$$\boldsymbol{x} \oplus_c \boldsymbol{y} = \frac{(1 + 2c\langle \boldsymbol{x}, \boldsymbol{y} \rangle + c\|\boldsymbol{y}\|^2)\boldsymbol{x} + (1 - c\|\boldsymbol{x}\|^2)\boldsymbol{y}}{1 + 2c\langle \boldsymbol{x}, \boldsymbol{y} \rangle + c^2\|\boldsymbol{x}\|^2\|\boldsymbol{y}\|^2}. \quad (1)$$

Exponential Map. For $\forall \boldsymbol{x} \in \mathbb{B}_c^n$, and $\forall \boldsymbol{v} \in \mathcal{T}_{\boldsymbol{x}}\mathbb{B}_c^n$ (*i.e.*, $\mathcal{T}_{\boldsymbol{x}}\mathbb{B}_c^n$ can be seen as Euclidean space), the exponential map $\exp_{\boldsymbol{x}}^c(\boldsymbol{v}) : \mathcal{T}_{\boldsymbol{x}}\mathbb{B}_c^n \to \mathbb{B}_c^n$ is described as follows:

$$\exp_{\boldsymbol{x}}^c(\boldsymbol{v}) = \boldsymbol{x} \oplus_c \frac{1}{\sqrt{c}} \tanh\left(\frac{\sqrt{c}\lambda_{\boldsymbol{x}}^c \|\boldsymbol{v}\|}{2}\right)[\boldsymbol{v}]. \quad (2)$$

Distance. For $\forall \boldsymbol{x}, \boldsymbol{y} \in \mathbb{B}_c^n$, the distance $d_c : \mathbb{B}_c^n \times \mathbb{B}_c^n \to \mathbb{R}$ is given by the following:

$$d_c(\boldsymbol{x}, \boldsymbol{y}) = \frac{2}{\sqrt{c}} \tanh^{-1}\left(\sqrt{c}\|-\boldsymbol{x} \oplus_c \boldsymbol{y}\|\right). \quad (3)$$

The distance between any point and the origin in the Poincaré Ball model indicates uncertainty of the point [4]. Specifically, there is a center in the ball. The hyperbolic distance from the embedding of each pixel to the origin (*i.e.*, the center of the ball) can serve as a measure of how confidently or certainly the pixel will be classified. When pixels are classified with high confidence, their embeddings should be far away from the center. By contrast, for pixels classified with high uncertainty, their embeddings are closer to the center of the ball. For example, in Fig. 2b, the hyperbolic distance of the pixel C is longer than that of the pixels A and B, indicating that the pixel C is classified more confidently.

IV. The Proposed Model

In this section, we first describe our proposed loss function and then detail the way to apply our loss to three recent semantic segmentation models.

A. The Proposed Loss Function

To clearly illustrate our proposed loss function, we firstly describe hyperbolic uncertainty again, then detail how to compute the uncertainty weight, and finally by combining cross-entropy loss with the uncertainty weight, provide the proposed Hyperbolic Uncertainty Loss (HyperUL). In addition, we also provide other variants of HyperUL.

Hyperbolic Uncertainty. As mentioned in the introduction, hyperbolic uncertainty can be used to measure the uncertainty of the segmentation result by computing the hyperbolic distance from the pixel embedding $\boldsymbol{x}$ to the origin $\mathbf{0}$. According to Eq. 3, the distance is given by the following:

$$d_c(\boldsymbol{x}, \mathbf{0}) = \frac{2}{\sqrt{c}} \tanh^{-1}\left(\sqrt{c}\|\boldsymbol{x}\|\right). \quad (4)$$

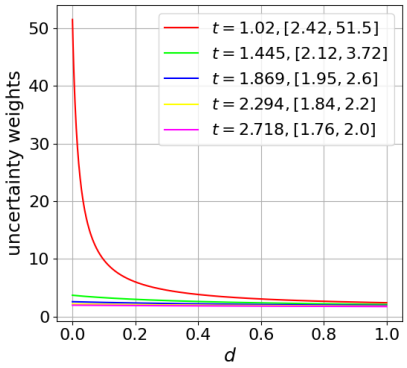

Fig. 3. The relationships between uncertainty weights and the hyper-parameter t.

The longer the distance is, the lower the uncertainty is.

Uncertainty Weight. In order to incorporate the hyperbolic uncertainty in the loss function, some transformations are needed. We firstly scale the distance to the interval $(0, 1]$ by diving by the largest distance $d_c(\boldsymbol{u}, \mathbf{0})$ in an image. $\boldsymbol{u}$ is the embedding of the most confidently classified pixel. Then the uncertainty weight is defined as follows:

$$\mathrm{uw}_{\boldsymbol{x}} = \frac{1}{\log(t + d)} + 1, \tag{5}$$

where, the scaled distance is $d = \frac{d_c(\boldsymbol{x}, \mathbf{0})}{d_c(\boldsymbol{u}, \mathbf{0})}$, and t is a hyper-parameter used to control the level of the uncertainty weights, and the default value is 1.02. Due to $\log_e 1 = 0$ and $\log_e e = 1$ and avoiding the 0 denominator, we choose five discrete values from the interval $[1.02, 2.718]$ for parameter analysis. As depicted in Fig. 3, smaller t provides bigger weights and wider variation range.

Cross Entropy Loss. According to the work [31], Cross Entropy Loss is defined as follows:

$$\mathrm{L}_{ce} = -w_k \log \frac{\exp(\boldsymbol{x}_k)}{\sum_{m=1}^{M} \exp(\boldsymbol{x}_m)}, \tag{6}$$

where k indicates the target class, w_k is the weight for the class k, and M is the number of classes. In Cross Entropy Loss, w_k is commonly used for class imbalance.

Hyperbolic Uncertainty Loss. By combining Eqs. 5 and 6, we provide the final Hyperbolic Uncertainty Loss (HyperUL) as follows:

$$\mathrm{HyperUL} = -(\mathrm{uw}_{\boldsymbol{x}})\ w_k \log \frac{\exp(\boldsymbol{x}_k)}{\sum_{m=1}^{M} \exp(\boldsymbol{x}_m)}. \tag{7}$$

This is a basic HyperUL, and we also provide various variants in the following content.

HyperUL-CE. We can directly utilize HyperUL (*i.e.*, Eq.7) to replace traditional cross-entropy loss. In this scenario, HyperUL is operated on each pixel in an entire image. Conversely, similar to Online Hard Example Mining (OHEM) [13], we can also put weights only on the most uncertain pixels. For example, we only put HyperUL on these pixels with top 70% uncertainty, while the rest of pixels continue to use the cross-entropy loss. For the ease of descriptions, we use the hyper-parameter h_r to indicate how uncertainly pixels are classified. The variant of HyperUL is defined as follows:

$$\text{HyperUL-CE} = \begin{cases} \text{HyperUL}, & d_c(\boldsymbol{x}, \mathbf{0}) \le d_c^{h_r}; \\ \mathrm{L}_{ce}, & \text{otherwise}, \end{cases} \tag{8}$$

where $d_c^{h_r} = d_c(\boldsymbol{x}, \mathbf{0}) + h_r \times (d_c(\boldsymbol{u}, \mathbf{0}) - d_c(\boldsymbol{x}, \mathbf{0}))$. The best h_r should be in $[0.3, 1]$. When $h_r = 1$, the variant HyperUL-CE becomes HyperUL. In Eq. 8, there exist two hyper-parameters t and h_r. Therefore, in the following ablation study V-C, we firstly provide parameter analysis results about t under the condition of $h_r = 1$. Then parameter analysis results about h_r are provided. These results are demonstrated in Tables III and IV, corresponding.

HyperUL-OHEM. As mentioned before, Hyperbolic uncertainty can be used to find not confidently classified pixels. Therefore, it can serve as a criterion to only select the highest-uncertainty pixels for back-propagation during training, which behaves like OHEM. In conventional OHEM, each pixel in an image is sorted by its loss, and only these pixels with higher loss values can be selected for back-propagation. The rest of pixels will be completely discarded, as these pixels are seen as easy examples. Similar to the criterion in conventional OHEM, we use the criterion of the higher uncertainties for HyperUL-OHEM instead of the criterion of the higher losses. The new criterion is given by the following:

$$\text{HyperUL-OHEM} = d_c(\boldsymbol{x}, \mathbf{0}) \le d_c^{o_r}, \tag{9}$$

where $d_c^{o_r} = d_c(\boldsymbol{x}, \mathbf{0}) + o_r \times (d_c(\boldsymbol{u}, \mathbf{0}) - d_c(\boldsymbol{x}, \mathbf{0}))$, and o_r is a hyper-parameter, which is used to select higher uncertain pixels for back-propagation. Similar to the settings in traditional OHEM, the o_r should be in $[0.3, 0.7]$. More parameter analysis results are illustrated in Table V. In addition, even though HyperUL-OHEM is totally different from HyperUL-CE, here we still use the name "HyperUL-OHEM" for this implementation for the ease of descriptions.

HyperUL-CE-OHEM. Combining HyperUL-CE and HyperUL-OHEM, we provide HyperUL-CE-OHEM. Specifically, there are two steps. The first step is to adopt HyperUL-CE to get losses of each pixels in a full image. Then, the next step is to utilize HyperUL-OHEM to pick top uncertain pixels for back-propagation. Also, there are three hyper-parameters, t, h_r, and o_r. In this application, we directly use the best parameters obtained from HyperUL-CE and HyperUL-OHEM to provide semantic segmentation performance.

B. Applications of HyperUL

In this subsection, we detail the way to apply the proposed HyperUL to recent semantic segmentation models, *e.g.*, SegFormer-B0 [14], STDC2-Seg50 [16], and BiSeNetV2 [15].

We first introduce how to transform the feature embeddings from Euclidean space into Hyperbolic space. Specifically, the output feature embeddings of the last layer of these segmentation models are directly converted by exponential map (*i.e.*, Eq. 2). For a given feature embedding $\boldsymbol{v}$ of a pixel in Euclidean space, the transformed one is as follows:

$$\exp_{\mathbf{0}}^{c}(\boldsymbol{v}) = \frac{1}{\sqrt{c}} \tanh\left(\sqrt{c}\,\|\boldsymbol{v}\|\right)[\boldsymbol{v}]. \tag{10}$$

After obtaining the feature embeddings in Hyperbolic space, the classical cross-entropy loss or cross-entropy loss combined with OHEM is directly replaced by our proposed HyperUL. Specifically, the cross-entropy loss adopted by SegFormer-B0 is directly substituted by HyperUL, and the cross-entropy loss together with OHEM used in BiSeNetV2 and STDC2-Seg50 is replaced by HyperUL.

V. Experiments

In this section, we first introduce the experimental settings, *i.e.*, employed semantic segmentation models, adopted datasets, and implementation details. Then we show our experimental results on two typical scene parsing datasets, *e.g.*, Cityscapes [1] and UAVid [11]. Finally, some ablation studies will be provided under different hyper-parameter settings. Please note that for the ease of the following descriptions, HyperUL and its variants are uniformly called "HyperUL".

A. Experimental Settings

Models. As mentioned in Section IV-B, SegFormer-B0 [14], STDC2-Seg50 [16], and BiSeNetV2 [15] are recently proposed lightweight and high-performance semantic segmentation approaches. As depicted in Section IV-A, the cross-entropy loss adopted by SegFormer-B0 will be replaced by our HyperUL during the training stage. Similarly, the cross-entropy loss together with the OHEM used in STDC2-Seg50 and BiSeNetV2 will be substituted by our HyperUL. We term these models with HyperUL as "SegFormer-B0+HyperUL", "STDC2-Seg50+HyperUL", and "BiSeNetV2+HyperUL", respectively. For fair comparisons, we train these models under the same settings, so their results are directly comparable.

Datasets. We conduct experiments on two publicly released datasets, *e.g.*, Cityscapes [1] and UAVid [11]. Cityscapes is a large semantic segmentation datasets, *i.e.*, 5000 fine annotated images with commonly used 19 classes, especially for the field of autonomous driving. This dataset is divided into 2975 training images, 500 validation images, and 1525 test images, respectively. All images are with the high resolution of 2048×1024. UAVid is also a high-resolution street scene semantic segmentation dataset while the images in it are collected by Unmanned Aerial Vehicles (UAV). There are two types of image resolutions, *i.e.*, 3840×2160 and 4096×2160. UAVid is comprised of 200 training images, 70 validation images, and 150 test images, respectively. Also, it has been densely labeled with 8 classes for the UAV-based semantic segmentation task.

Implementation Details. We train all models on a server with 4 Tesla A100 GPUs. We initialize the backbones of SegFormer-B0(+HyperUL), and STDC2-Seg50(+HyperUL) with corresponding pretrained models on the Imagenet-1K dataset, while same as previous work [15], BiSeNetV2(+HyperUL) is trained from scratch. When training these models, we adopt multiple data augmentation techniques [14], [16], such as Random Resize with the ratio of $[0.5, 2.0]$, Random Horizontal Flipping, and Random Cropping to 1024×512 for both Cityscapes and UAVid. Besides, the batch size for SegFormer-B0(+HyperUL), STDC2-Seg50(+HyperUL), and BiSeNetV2(+HyperUL) is set as 32 on both datasets. We utilize AdamW optimizer [32] with initial learning rate of 0.00015 for the encoder module and 0.0015 for the decoder module for SegFormer-B0(+HyperUL), and we set 0.0015 for BiSeNetV2(+HyperUL) and STDC2-Seg50(+HyperUL). As commonly used configuration, Polynomial Learning Rate Decay Scheduler with the power of 0.9 is used. In addition, we train all models for 80K iterations on both datasets, and adopt the warmup trick for the first 1K iterations. Finally, we use mIoU to evaluate the segmentation performance.

TABLE II
Comparison results between SegFormer-B0, STDC2-Seg50, BiSeNetV2 and corresponding counterparts with HyperUL on the Cityscapes and UAVid test data sets. SS means the single-scale test. MSCF means multi-scale, cropping, and flipping test. MIOU means mean Intersection over Union.

	Cityscapes SS/MSCF (mIoU)	UAVid SS/MSCF(mIoU)
SegFormer-B0	74.1 / 77.0	67.2 / 68.7
SegFormer-B0+HyperUL	**74.8 / 77.1**	**67.7 / 69.2**
STDC2-Seg50	70.4 / 73.5	67.6 / 69.4
STDC2-Seg50+HyperUL	**72.7 / 75.7**	**68.2 / 70.1**
BiSeNetV2	72.4 / 74.7	67.0 / 68.0
BiSeNetV2+HyperUL	**72.6 / 74.7**	**67.3 / 68.6**

B. Quantitative and Qualitative Analysis

In this subsection, we provide quantitative comparisons on the Cityscapes and UAVid test datasets, respectively. Also we provide some qualitative analysis on the Cityscapes and UAVid validation datasets.

Quantitative Comparisons. Similar to works [14]–[16], we train all models on both the training and validation datasets, and then test them on the test datasets. As depicted in Table II, SegFormer-B0+HyperUL, STDC2-Seg50+HyperUL, and BiSeNetV2+HyperUL consistently achieve segmentation performance improvement on both Cityscapes and UAVid test datasets compared with their counterparts. Specifically, the improvements for these segmentation models equipped with HyperUL are 0.7, 2.3, and 0.2 respectively on the Cityscapes test dataset for the single-scale test, and the improvements are 0.5, 0.6, and 0.3 respectively on the UAVid test dataset. This means that our proposed HyperUL has an outstanding ability to attract models to useful pixels (*i.e.*, pixels with larger uncertainty) during training.

Qualitative Analysis. Here we visualize segmentation results and corresponding uncertainty images over iterations on images from the Cityscapes and UAVid validation datasets in Figs. 4 and 5. On each uncertainty image, uncertain pixels with top 95% uncertainty are showed. These pixels are highlighted by black and green colors. As demonstrated in Fig. 4, we see that from the second column to the forth column, the number of uncertain pixels is gradually decreasing. This means that HyperUL encourages segmentation models to learn knowledge from useful pixels (*i.e.*, with larger uncertainty). The Fig. 5 shows similar results.

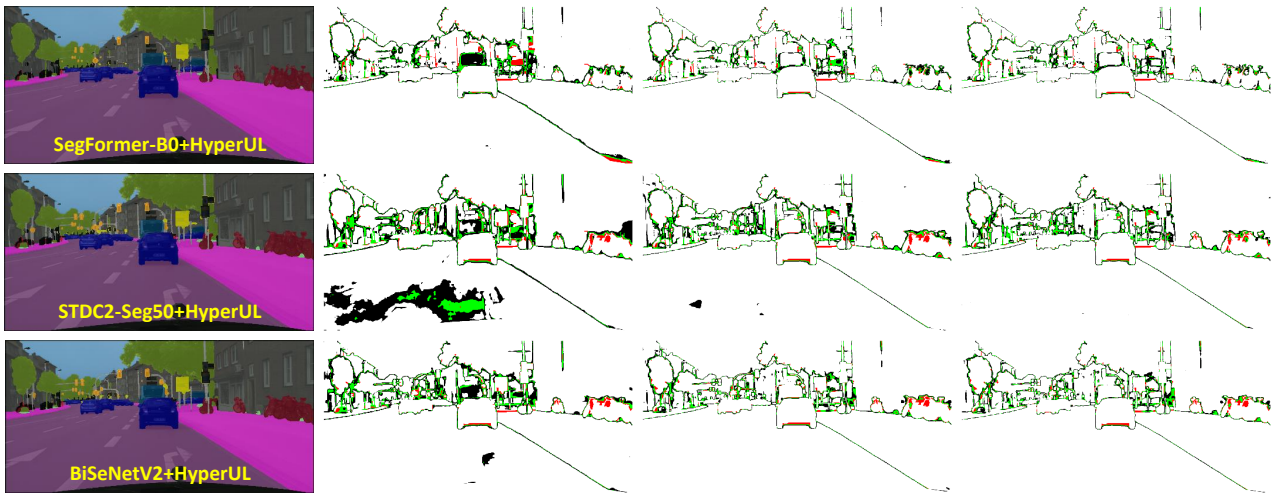

Fig. 4. Uncertainty evolution over iterations on the Cityscapes validation dataset. Same as before, black, red, and green color pixels represent uncertain pixels, misclassified pixels, and highly uncertain-misclassified pixels, respectively. All images in the first column are segmented results of three models. For SegFormer-B0+HyperUL, STDC2-Seg50+HyperUL, and BiSeNetV2+HyperUL, uncertainty images in the second, third, and fourth columns are generated under 100, 500, and the last epoch. (**Best viewed in color.**)

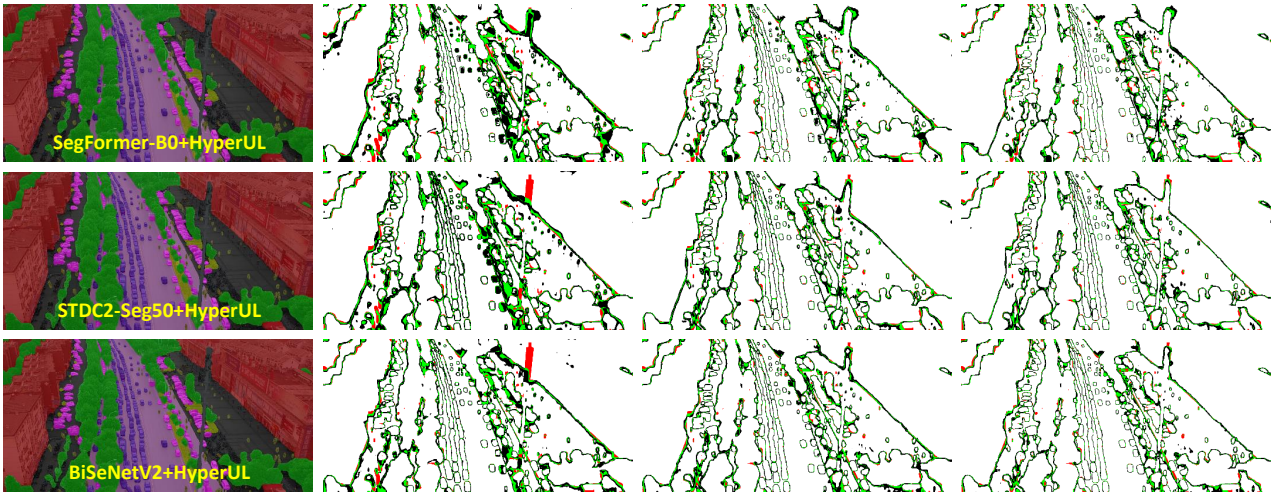

Fig. 5. Uncertainty evolution over iterations on the UAVid validation dataset. Same as before, black, red, and green color pixels represent uncertain pixels, misclassified pixels, and highly uncertain-misclassified pixels, respectively. All images in the first column are segmented results of three models. For SegFormer-B0+HyperUL, STDC2-Seg50+HyperUL, and BiSeNetV2+HyperUL, uncertainty images in the second, third, and fourth columns are generated under 100, 500, and the last epoch. (**Best viewed in color.**)

More segmentation results on both validation datasets are shown in Figs. 6, 7, 8, and 9. As indicated by white rectangles and circles, the regions segmented by segmentation models with HyperUL are more coherent and complete than their counterparts.

C. Ablation Study

This subsection illustrates ablation experiments to compare the effectiveness of HyperUL and its variants. Also these experiments help find the best hyper-parameters of the proposed loss function. Here, all ablation experiments adopt SegFormer-B0 [14] and are conducted on the Cityscapes [1] dataset. Experimental settings are same as that in Section V-A. In the following content, we first try to find hyper-parameters t and h_r for HyperUL-CE. Then we try to find the best o_r for HyperUL-OHEM. Finally, we provide segmentation result for HyperUL-CE-OHEM with searched t, h_r, and o_r, as well as show comparison results with conventional cross-entropy loss and cross-entropy loss with OHEM.

TABLE III
SENSITIVITY ANALYSIS FOR THE PARAMETER t ON THE CITYSCAPES VALIDATION SET WITH h_r FIXED TO 1.

t	1.02	1.445	1.869	2.294	2.718
mIoU	74.4	73.9	74.4	**74.5**	74.4

HyperUL-CE with Parameter t. As described in Eq. 5, the hyper-parameter t is used to control the scale of the uncertainty weights. The default is 1.02. As shown in Fig. 3, when t becomes bigger, the uncertainty weights will be smaller, and the dynamic range of weight for each pixel also becomes limited. For example, when $t = 1.02$, the wide range of weight is from 2.42 to 51.5. In contrast,

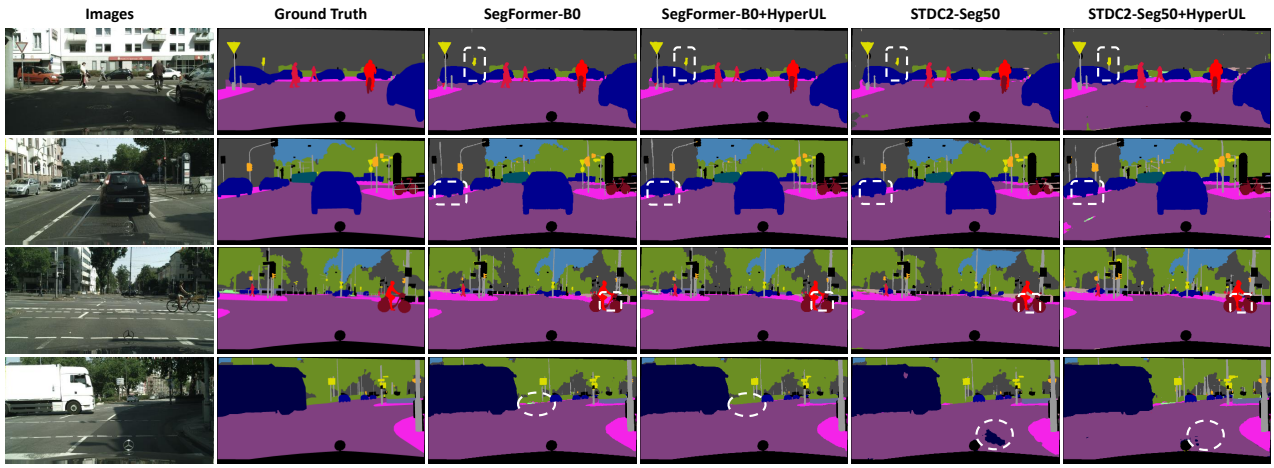

Fig. 6. Qualitative segmentation examples of SegFormer-B0(+HyperUL) and STDC2-Seg50(+HyperUL) on the Cityscapes validation dataset. As indicated by white rectangles and circles, the regions segmented by SegFormer-B0+HyperUL and STDC2-Seg50+HyperUL are more coherent and complete than SegFormer-B0 and STDC2-Seg50. (**Best viewed in color.**)

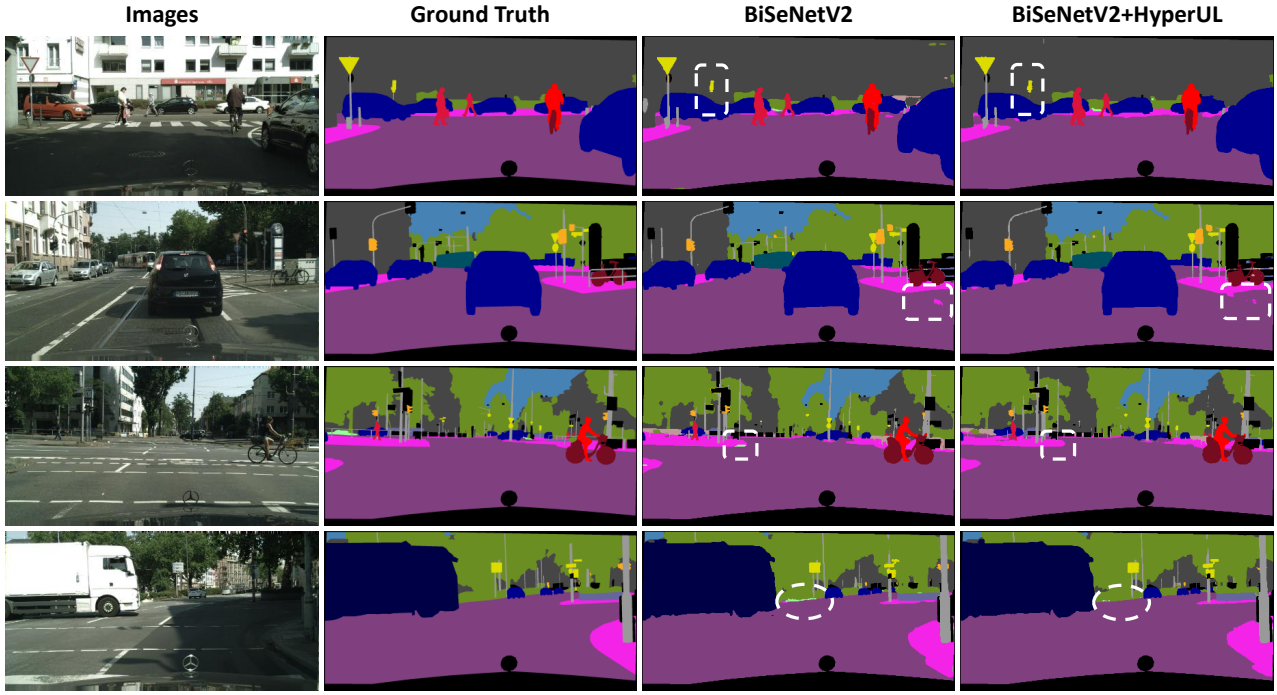

Fig. 7. Qualitative segmentation examples of BiSeNetV2(+HyperUL) on the Cityscapes validation dataset. As indicated by white rectangles and circles, the regions segmented by BiSeNetV2+HyperUL are more coherent and complete than BiSeNetV2. (**Best viewed in color.**)

when $t = 2.718$, the narrow range of weight is only from 1.76 to 2.0. we will conduct comparison experiments with $t = \{1.02, 1.445, 1.869, 2.294, 2.718\}$ under the condition of $h_r = 1$. Parameter analysis results are shown in Table III. We see that when $t = 2.294$, SegFormer-B0+HyperUL-CE (t) obtains the best segmentation performance.

HyperUL-CE with Parameter h_r. As introduced in HyperUL-CE, parameter h_r indicates how uncertainly a pixel will be identified. This can be adopted to control which pixel will be weighted by the corresponding uncertainty weight. The h_r could be in the range of $[0.3, 1]$. Here we set $h_r = \{0.3, 0.5, 0.7, 0.9, 1\}$ with t fixed to 2.294. Parameter analysis results are provided in Table IV. We see that when $h_r = 1$, SegFormer-B0+HyperUL-CE (h_r) gets the best segmentation result. This means that considering uncertainties for all pixels in an image is beneficial for performance improvement.

TABLE IV
SENSITIVITY ANALYSIS FOR THE PARAMETER h_r ON THE CITYSCAPES VALIDATION SET WITH t FIXED TO 2.294.

h_r	0.3	0.5	0.7	0.9	1
mIoU	74.4	73.8	74.1	74.2	**74.5**

HyperUL-OHEM with Parameter o_r. As described in HyperUL-OHEM, o_r is utilized to decide that these pixels with top uncertainty will be used for back-propagation. As

Fig. 8. Qualitative segmentation examples of SegFormer-B0(+HyperUL) and STDC2-Seg50(+HyperUL) on the UAVid validation dataset. We see that the regions segmented by SegFormer-B0+HyperUL and STDC2-Seg50+HyperUL are more coherent and complete than SegFormer-B0 and STDC2-Seg50. (**Best viewed in color.**)

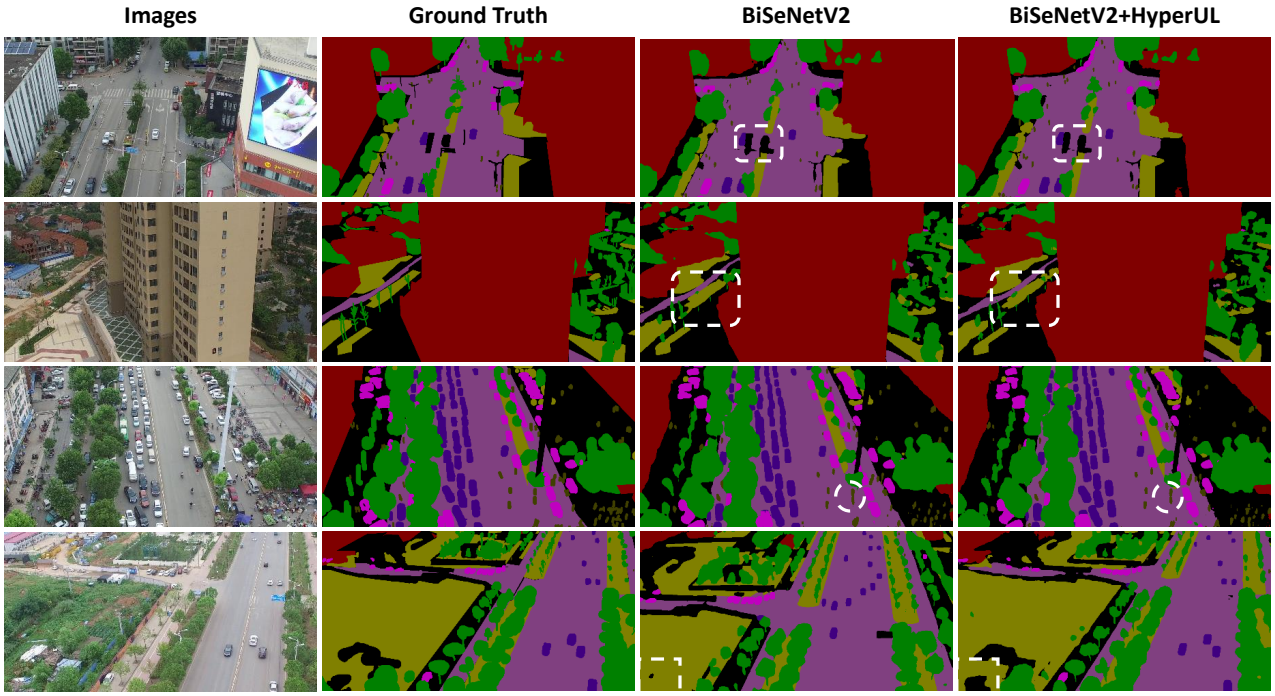

Fig. 9. Qualitative segmentation examples of BiSeNetV2(+HyperUL) on the UAVid validation dataset. We see that the regions segmented by BiSeNetV2+HyperUL are more coherent and complete than BiSeNetV2. (**Best viewed in color.**)

TABLE V
SENSITIVITY ANALYSIS FOR THE PARAMETER o_r ON THE CITYSCAPES VALIDATION SET.

o_r	0.3	0.4	0.5	0.6	0.7
mIoU	72.6	73.2	74.4	**74.5**	74.3

o_r becomes bigger, more uncertain pixels will be selected for back-propagation. Here, we set $o_r = \{0.3, 0.4, 0.5, 0.6, 0.7\}$ for sensitivity analysis. Parameter analysis results are depicted in Table V. We observe that when $o_r = 0.6$, SegFormer-B0+HyperUL-OHEM (o_r) obtains the best segmentation performance. This result is almost the same as that of SegFormer-B0+HyperUL-CE.

HyperUL-CE-OHEM with Parameters t, h_r, and o_r. As mentioned before, HyperUL-CE-OHEM is the combination of HyperUL-CE and HyperUL-OHEM. Here, since hyper-parameters t, h_r, and o_r have been searched before, we directly provide the segmentation result with the best parameters $t = 2.294$, $h_r = 1$, and $o_r = 0.6$. The experimental result on the Cityscapes validation set is 74.4 mIoU, which is worse than SegFormer-B0+HyperUL-CE and SegFormer-B0+HyperUL-OHEM results.

Comparisons with conventional CE and CE-OHEM. To compare our proposed HyperUL and its variants with conventional cross-entropy loss and cross-entropy loss with

TABLE VI
COMPARISONS WITH CONVENTIONAL CROSS ENTROPY LOSS (CE) AND CE WITH ONLINE HARD EXAMPLE MINING (OHEM) ON THE CITYSCAPES VALIDATION SET.

Losses	mIoU (%)
CE	72.9
CE-OHEM (0.7)	73.7
HyperUL-CE (t)	74.5
HyperUL-CE (h_r)	74.5
HyperUL-OHEM (o_r)	74.5
HyperUL-CE-OHEM (t, h_r, o_r)	74.4

OHEM, we directly provide comparison results in Table VI. The segmentation results on the Cityscapes validation dataset reveal that our proposed loss function is superior to conventional CE and OHEM.

VI. CONCLUSION

"Hyperbolic Uncertainty Loss" (HyperUL) was proposed in this work to handle underlying hierarchical structures of segmentation datasets and uncertainties. To the best of our knowledge, this is the first work to apply the property of Hyperbolic space to the supervised semantic segmentation task. In addition, we detailed different types of HyperUL, such as HyperUL-CE, HyperUL-OHEM, and HyperUL-CE-OHEM, as well as applied them to recently representative segmentation models. By employing the proposed HyperUL, existing segmentation models consistently obtain additional performance improvement. Moreover, our loss function HyperUL is general in nature and has the potential to be applied to other applications such as 3D point cloud segmentation, medical image segmentation, etc.

ACKNOWLEDGMENTS

The authors would like to thank the Finnish UAV Ecosystem (No. 338080) and RoboMesh (No. 336060) projects for the financial support. In addition, the authors wish to acknowledge CSC–IT Center for Science, Finland, for computational resources.

REFERENCES

[1] M. Cordts, M. Omran, S. Ramos, T. Rehfeld, M. Enzweiler, R. Benenson, U. Franke, S. Roth, and B. Schiele, "The Cityscapes Dataset for Semantic Urban Scene Understanding," in *Computer Vision and Pattern Recognition*, 2016, pp. 3213–3223.

[2] A. Milioto, P. Lottes, and C. Stachniss, "Real-time semantic segmentation of crop and weed for precision agriculture robots leveraging background knowledge in cnns," in *International Conference on Robotics and Automation*, 2018, pp. 2229–2235.

[3] B. Chen, C. Gong, and J. Yang, "Importance-aware semantic segmentation for autonomous vehicles," *IEEE Transactions on Intelligent Transportation Systems*, vol. 20, no. 1, pp. 137–148, 2019.

[4] V. Khrulkov, L. Mirvakhabova, E. Ustinova, I. Oseledets, and V. Lempitsky, "Hyperbolic image embeddings," in *Computer Vision and Pattern Recognition*, 2020, pp. 6418–6428.

[5] Y. Gal and Z. Ghahramani, "Dropout as a Bayesian approximation: Representing model uncertainty in deep learning," in *International Conference on Machine Learning*, 2016.

[6] B. Lakshminarayanan, A. Pritzel, and C. Blundell, "Simple and scalable predictive uncertainty estimation using deep ensembles," in *Neural Information Processing Systems*, vol. 30, 2017.

[7] M. Valdenegro-Toro, "Deep sub-ensembles for fast uncertainty estimation in image classification," *arXiv preprint arXiv:1910.08168*, 2019.

[8] B. Bischke, P. Helber, D. Borth, and A. Dengel, "Segmentation of imbalanced classes in satellite imagery using adaptive uncertainty weighted class loss," in *IGARSS 2018-2018 IEEE International Geoscience and Remote Sensing Symposium*. IEEE, 2018, pp. 6191–6194.

[9] P. O. Bressan, J. M. Junior, J. A. C. Martins, D. N. Gonçalves, D. M. Freitas, L. P. Osco, J. d. A. Silva, Z. Luo, J. Li, R. C. Garcia *et al.*, "Semantic segmentation with labeling uncertainty and class imbalance," *arXiv preprint arXiv:2102.04566*, 2021.

[10] N. Linial, E. London, and Y. Rabinovich, "The geometry of graphs and some of its algorithmic applications," *Combinatorica*, vol. 15, no. 2, pp. 215–245, 1995.

[11] Y. Lyu, G. Vosselman, G.-S. Xia, A. Yilmaz, and M. Y. Yang, "Uavid: A semantic segmentation dataset for uav imagery," *ISPRS Journal of Photogrammetry and Remote Sensing*, vol. 165, pp. 108 – 119, 2020.

[12] W. Peng, T. Varanka, A. Mostafa, H. Shi, and G. Zhao, "Hyperbolic deep neural networks: A survey," *IEEE Transactions on Pattern Analysis and Machine Intelligence*, 2021.

[13] A. Shrivastava, A. Gupta, and R. Girshick, "Training region-based object detectors with online hard example mining," in *Computer Vision and Pattern Recognition*, 2016, pp. 761–769.

[14] E. Xie, W. Wang, Z. Yu, A. Anandkumar, J. M. Alvarez, and P. Luo, "Segformer: Simple and efficient design for semantic segmentation with transformers," *arXiv preprint arXiv:2105.15203*, 2021.

[15] C. Yu, C. Gao, J. Wang, G. Yu, C. Shen, and N. Sang, "Bisenet v2: Bilateral network with guided aggregation for real-time semantic segmentation," *International Journal of Computer Vision*, pp. 1–18, 2021.

[16] M. Fan, S. Lai, J. Huang, X. Wei, Z. Chai, J. Luo, and X. Wei, "Rethinking bisenet for real-time semantic segmentation," in *Computer Vision and Pattern Recognition*, 2021, pp. 9716–9725.

[17] H. Li, P. Xiong, H. Fan, and J. Sun, "Dfanet: Deep feature aggregation for real-time semantic segmentation," in *Computer Vision and Pattern Recognition*, 2019, pp. 9522–9531.

[18] C. Yu, J. Wang, C. Peng, C. Gao, G. Yu, and N. Sang, "Bisenet: Bilateral segmentation network for real-time semantic segmentation," in *European Conference on Computer Vision*, 2018, pp. 334–349.

[19] S. Zheng, J. Lu, H. Zhao, X. Zhu, Z. Luo, Y. Wang, Y. Fu, J. Feng, T. Xiang, P. H. Torr *et al.*, "Rethinking semantic segmentation from a sequence-to-sequence perspective with transformers," in *Computer Vision and Pattern Recognition*, 2021, pp. 6881–6890.

[20] Z. Liu, Y. Lin, Y. Cao, H. Hu, Y. Wei, Z. Zhang, S. Lin, and B. Guo, "Swin transformer: Hierarchical vision transformer using shifted windows," *arXiv preprint arXiv:2103.14030*, 2021.

[21] Y. Yuan, R. Fu, L. Huang, W. Lin, C. Zhang, X. Chen, and J. Wang, "Hrformer: High-resolution transformer for dense prediction," *arXiv preprint arXiv:2110.09408*, 2021.

[22] J. Wang, K. Sun, T. Cheng, B. Jiang, C. Deng, Y. Zhao, D. Liu, Y. Mu, M. Tan, X. Wang *et al.*, "Deep high-resolution representation learning for visual recognition," *IEEE transactions on pattern analysis and machine intelligence*, 2020.

[23] O.-E. Ganea, G. Bécigneul, and T. Hofmann, "Hyperbolic neural networks," in *Neural Information Processing Systems*, 2018.

[24] R. Shimizu, Y. Mukuta, and T. Harada, "Hyperbolic neural networks++," in *International Conference on Learning Representations*, 2021.

[25] J. Yan, L. Luo, C. Deng, and H. Huang, "Unsupervised hyperbolic metric learning," in *Computer Vision and Pattern Recognition*, 2021, pp. 12 465–12 474.

[26] J. Hsu, J. Gu, G.-H. Wu, W. Chiu, and S. Yeung, "Learning hyperbolic representations for unsupervised 3d segmentation," *arXiv preprint arXiv:2012.01644*, 2020.

[27] J. Gawlikowski, C. R. N. Tassi, M. Ali, J. Lee, M. Humt, J. Feng, A. Kruspe, R. Triebel, P. Jung, R. Roscher *et al.*, "A survey of uncertainty in deep neural networks," *arXiv preprint arXiv:2107.03342*, 2021.

[28] A. Kendall and Y. Gal, "What uncertainties do we need in bayesian deep learning for computer vision?" in *Neural Information Processing Systems*, vol. 30, 2017.

[29] M. Sensoy, L. Kaplan, and M. Kandemir, "Evidential deep learning to quantify classification uncertainty," in *Neural Information Processing Systems*, vol. 31, 2018.

[30] A. A. Ungar, "A gyrovector space approach to hyperbolic geometry," *Synthesis Lectures on Mathematics and Statistics*, vol. 1, no. 1, pp. 1–194, 2008.

[31] P.-T. de Boer, D. P. Kroese, S. Mannor, and R. Y. Rubinstein, "A tutorial on the cross-entropy method," *Annals of Operations Research*, vol. 134, pp. 19–67, 2005.

[32] I. Loshchilov and F. Hutter, "Decoupled weight decay regularization," in *International Conference on Learning Representations*, 2019.